

# Dynamic NHERF interaction with TRPC4/5 proteins is required for channel gating by diacylglycerol

Ursula Storch<sup>a,1</sup>, Anna-Lena Forst<sup>a,1</sup>, Franziska Pardatscher<sup>a</sup>, Serap Erdogmus<sup>a</sup>, Maximilian Philipp<sup>a</sup>, Manuel Gregoritz<sup>a</sup>, Michael Mederos y Schnitzler<sup>a,b,2</sup>, and Thomas Gudermann<sup>a,b,c</sup>

<sup>a</sup>Walther Straub Institute of Pharmacology and Toxicology, Ludwig Maximilian University of Munich, 80336 Munich, Germany; <sup>b</sup>German Centre for Cardiovascular Research, Munich Heart Alliance, 80802 Munich, Germany; and <sup>c</sup>Comprehensive Pneumology Center Munich, German Center for Lung Research, 81377 Munich, Germany

Edited by David E. Clapham, Howard Hughes Medical Institute, Boston Children's Hospital, Boston, MA, and approved November 30, 2016 (received for review July 27, 2016)

**The activation mechanism of the classical transient receptor potential channels TRPC4 and -5 via the G<sub>q/11</sub> protein-phospholipase C (PLC) signaling pathway has remained elusive so far. In contrast to all other TRPC channels, the PLC product diacylglycerol (DAG) is not sufficient for channel activation, whereas TRPC4/5 channel activity is potentiated by phosphatidylinositol 4,5-bisphosphate (PIP<sub>2</sub>) depletion. As a characteristic structural feature, TRPC4/5 channels contain a C-terminal PDZ-binding motif allowing for binding of the scaffolding proteins Na<sup>+</sup>/H<sup>+</sup> exchanger regulatory factor (NHERF) 1 and 2. PKC inhibition or the exchange of threonine for alanine in the C-terminal PDZ-binding motif conferred DAG sensitivity to the channel. Altogether, we present a DAG-mediated activation mechanism for TRPC4/5 channels tightly regulated by NHERF1/2 interaction. PIP<sub>2</sub> depletion evokes a C-terminal conformational change of TRPC5 proteins leading to dynamic dissociation of NHERF1/2 from the C terminus of TRPC5 as a prerequisite for DAG sensitivity. We show that NHERF proteins are direct regulators of ion channel activity and that DAG sensitivity is a distinctive hallmark of TRPC channels.**

diacylglycerol | NHERF | TRPC | PIP<sub>2</sub> depletion | protein interaction

**T**RPC4 and -5 channels are members of the classical transient receptor potential cation (TRPC) family of nonselective, calcium permeable receptor-operated cation channels. They are widely expressed in many tissues, including brain, kidney, and the vascular system. High expression levels are found in the central nervous system where TRPC4 and -5 are involved in amygdala function and fear-related behavior (1, 2), seizure, and excitotoxicity (3). Furthermore, TRPC5 channels are implicated in neuronal depolarization and bursting during epileptiform seizures (4) and regulate hippocampal neurite length and growth cone morphology (5). In the kidney, TRPC5 channels are proposed to be protective against renal failure (6). TRPC channels are usually activated by G<sub>q/11</sub> protein-coupled receptors via phospholipase C (PLC) activation resulting in cleavage of phosphatidylinositol-3,4-bisphosphate (PIP<sub>2</sub>) into the second messengers inositol-1,4,5-trisphosphate (IP<sub>3</sub>) and diacylglycerol (DAG). DAG is known to activate TRPC2, -3, -6, and -7 (7–9) channels, whereas TRPC4 and -5 are supposed to be insensitive to the PLC product DAG (8) and are even inhibited by DAG or its membrane-permeable analog 1-oleoyl-2-acetyl-sn-glycerol (OAG) (10). DAG-mediated TRPC5 channel inhibition was shown to be PKC dependent (10). Furthermore, TRPC4 and -5 channels can be activated by depleting PIP<sub>2</sub> (11, 12), contrary to TRPC6 and -7 channels, which are inhibited by PIP<sub>2</sub> depletion (13). However, there are first hints to show that endogenously expressed TRPC5 channels might be DAG sensitive (14) but mechanistic insight is lacking so far.

A noteworthy structural difference between TRPC4 and -5 and the established DAG-sensitive TRPC3, -6, and -7 channels is the PDZ-binding motif VTTLR in the C termini of TRPC4 and -5 channels (15–17) as a structural basis of the interaction with Na<sup>+</sup>/H<sup>+</sup> exchanger regulatory factor (NHERF) proteins. Interestingly, the latter binding motif also contains a PKC phosphorylation site known to be crucial

for TRPC5 desensitization subsequent to receptor activation (18). The adaptor proteins NHERF1 and -2 are structurally closely related, form homo- and heterodimers (19), and are characterized by two tandem PDZ domains and a C-terminal domain that allows for association with the actin cytoskeleton via interaction with members of the ezrin/radixin/moesin (ERM) family (17). Thus, NHERF1 and -2 proteins are thought to serve as adaptors to link integral membrane proteins to the cytoskeleton. Maintenance of the subcellular architecture by NHERF proteins is critical for salient cell functions, for example in the kidney, small intestine, and other organs, where they interact with transporters, ion channels, signaling proteins, transcription factors, enzymes, G protein-coupled receptors (GPCRs), and tyrosine kinase receptors (20–24). NHERF proteins regulate phosphate transport in proximal tubule cells (25), are involved in ion transport in the small intestine (26), and regulate the activity of the glutamate transporter GLAST and of the metabolic glutamate receptor mGlu5 in astrocytes (27, 28). Moreover, they play a role in cell growth and cancer (29–31). Coimmunoprecipitation (17, 32) and electrophysiological experiments (16) showed that NHERF1 and -2 interact with TRPC4 and -5. However, it is not known whether this protein–protein interaction only serves a structural role or whether there are functional consequences with regard to channel function as well. Moreover, the exact signaling pathway linking G<sub>q/11</sub>-coupled receptors with activation of TRPC4 and -5 is largely obscure. Here,

## Significance

**Transient receptor potential cation (TRPC) 4 and 5 channels are nonselective cation channels activated via G protein-coupled receptors. In contrast to all other TRPC channels, they are regarded as insensitive to the phospholipase C (PLC) product diacylglycerol (DAG). Deeper insight into the G protein-dependent activation mechanism of TRPC4/5 channels is lacking. In this study we unravel the G<sub>q/11</sub> protein-mediated signaling pathway leading to TRPC4/5 activation. Depletion of phosphatidylinositol 4,5-bisphosphate causes a conformational change of the TRPC5 C terminus leading to dissociation of Na<sup>+</sup>/H<sup>+</sup> exchanger regulatory factor (NHERF) proteins thereby inducing a DAG-sensitive channel state. Our findings reveal a previously unidentified activation mechanism of TRPC4/5 channels with NHERF proteins as dynamic regulators of channel activity. Moreover, we demonstrate that TRPC channels are DAG sensitive.**

Author contributions: U.S., A.-L.F., M.M.y.S., and T.G. designed research; U.S., A.-L.F., F.P., S.E., M.P., M.G., and M.M.y.S. performed research; U.S., A.-L.F., F.P., S.E., M.G., and M.M.y.S. analyzed data; and U.S., M.M.y.S., and T.G. wrote the paper.

The authors declare no conflict of interest.

This article is a PNAS Direct Submission.

Freely available online through the PNAS open access option.

<sup>1</sup>U.S. and A.-L.F. have contributed equally to this work.

<sup>2</sup>To whom correspondence should be addressed. Email: mederos@lrz.uni-muenchen.de.

This article contains supporting information online at [www.pnas.org/lookup/suppl/doi:10.1073/pnas.1612263114/-DCSupplemental](http://www.pnas.org/lookup/suppl/doi:10.1073/pnas.1612263114/-DCSupplemental).

we offer a paradigm with the potential to integrate seemingly opposing theories of TRPC4 and -5 channel gating and identify dynamic NHERF-TRPC5 channel interactions as a crucial step for channel activation by PLC-linked receptors.

## Results

**OAG Increases TRPC5 Currents, if Phosphorylation by PKC Is Prevented.** To investigate whether TRPC5 channels are DAG sensitive, we performed electrophysiological whole-cell measurements with HEK293 cells transiently expressing TRPC5. Application of the membrane-permeable DAG analog OAG did not elicit TRPC5 currents, but rather resulted in small current decreases reaching a nadir after 60 s (Fig. 1A) in line with observations by Venkatachalam et al. (10). A total of 300  $\mu$ M LaCl<sub>3</sub> (Fig. 1A) or acidic bath solutions with pH 6.5 (33) (SI Appendix, Fig. S1A) served as positive control for TRPC5 expression and consistently led to significant TRPC5 current increases. Accumulation of endogenous DAG by application of the DAG kinase inhibitor RHC-80267 (Fig. 1B) or the DAG lipase inhibitor R59949 (SI Appendix, Fig. S1B) did not result in increased TRPC5 currents, whereas activation of endogenous muscarinic receptors by carbachol evoked significant TRPC5 currents. Notably, untransfected or en-

hanced (e)GFP-expressing HEK293 cells showed no current changes upon OAG application (SI Appendix, Fig. S1C and D). Next, TRPC5-expressing cells were incubated with the selective PKC inhibitor bisindolylmaleimide I (BIM I) for 15 min (Fig. 1C), resulting in significantly increased OAG-induced TRPC5 currents. The less selective PKC inhibitor staurosporine had a similar effect (Fig. 1D). Carbachol served as a positive control for these experiments. Moreover, application of OAG- to eGFP-expressing HEK293 preincubated with BIM I did not elicit increased currents, suggesting that endogenously expressed channels are not involved (SI Appendix, Fig. S1E). In contrast, protein kinase A inhibition by H89 did not lead to DAG sensitivity of TRPC5 (SI Appendix, Fig. S1F).

To further define the role of PKC for the OAG sensitivity of TRPC5, we exchanged threonine at position 972 for alanine in the PDZ-binding motif of TRPC5 (V1<sup>972</sup>-TRL→VA<sup>972</sup>-TRL). T<sup>972</sup> represents a putative PKC phosphorylation site known to regulate TRPC5 current inhibition after agonist stimulation (18). Surprisingly, the latter amino acid exchange conferred OAG sensitivity upon TRPC5 (Fig. 1D). OAG elicited rapidly decaying transient TRPC5 currents, whereas carbachol stimulation did not entail any current decay concordant with observations by Zhu et al. (18). A permanent phosphorylation status was mimicked by replacing T<sup>972</sup> by aspartate (T972D, Fig. 1E) or glutamate (T972E, SI Appendix, Fig. S24). Both TRPC5 mutants were resistant to OAG. Instead, they showed small outward current decreases after OAG application similar to wild-type TRPC5 channels. In these experiments LaCl<sub>3</sub> was used as a positive control (34) for functional TRPC5 expression. Moreover, incubation of TRPC5-T972E-expressing HEK293 cells with BIM I (SI Appendix, Fig. S2B) did not give rise to OAG-induced currents, supporting the idea that dephosphorylation of threonine 972 might contribute to the activation of TRPC5 channels by DAG.

## C-Terminal NHERF Interaction Determines OAG Sensitivity of TRPC5.

Because T<sup>972</sup> is part of the PDZ-binding motif, the structural basis of NHERF interaction, we next analyzed the role of NHERF binding for the DAG sensitivity of TRPC5. For this, we used shRNAs directed against NHERF1 or -2 in TRPC5-expressing HEK293 cells. By quantitative RT-PCR (qRT-PCR), we noted that HEK293 cells endogenously express high mRNA levels of NHERF1 and threefold lower mRNA levels of NHERF2 (SI Appendix, Fig. S3A), both of which were efficiently down-regulated by NHERF1 and -2 shRNAs. Additionally, down-regulation of NHERF proteins was confirmed at the protein level (SI Appendix, Fig. S3A-C). As expected, HEK293 cells transfected with TRPC5 and unrelated control shRNA were not OAG sensitive (Fig. 2A). However, cells transfected with TRPC5 and shRNA directed against NHERF1 (Fig. 2B) or NHERF2 (Fig. 2C) became OAG sensitive. Cotransfection with both shRNAs had no additive effect (SI Appendix, Fig. S4A). LaCl<sub>3</sub> served as positive control for functional TRPC5 expression. These findings support the notion that the interaction of NHERF1 and -2 proteins with the C terminus of TRPC5 determines the OAG sensitivity of TRPC5. Coexpression of NHERF1 and TRPC5 in HEK293 cells did not render the ion channel OAG responsive (Fig. 2). Moreover, cells were cotransfected with TRPC5 and a NHERF1 mutant with an amino acid exchange of glutamate to alanine in the first PDZ domain (NHERF1-E68A). This mutation was first identified in a patient with inappropriate renal phosphate reabsorption (35). Concordant with our hypothesis, coexpression of NHERF1-E68A caused OAG sensitivity of TRPC5 (Fig. 2E). Because the PDZ1 domain of NHERF1 is essential for the interaction with TRPC4 and -5, these were interpreted to mean that NHERF1-E68A is unable to bind to TRPC5. Of note, endogenous NHERF1 proteins in NHERF1-E68A-coexpressing cells did not prevent OAG sensitivity of TRPC5, probably due to the capacity of NHERF1 proteins to form dimers (19) composed of NHERF1-E68A and endogenous NHERF1 unable to interact with TRPC5. Coexpression of NHERF1-E68A and TRPC5-T972E also resulted in OAG sensitivity (SI Appendix, Fig. S4B). To investigate whether

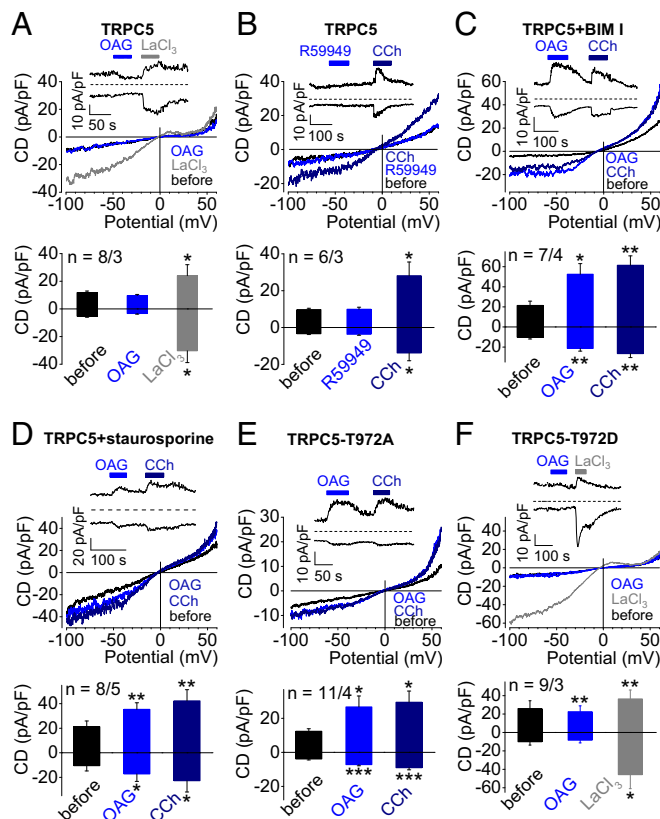


**Fig. 1.** OAG increases TRPC5 currents, if phosphorylation by PKC is prevented. (A–E) Whole-cell recordings of HEK293 cells expressing TRPC5 (A–D), TRPC5-T972A (E), or TRPC5-T972D (F) with representative current density (CD) voltage curves, CD time courses, and summaries of CDs at holding potentials of  $\pm 60$  mV are displayed. Stippled lines indicate zero currents. Applications of 100  $\mu$ M OAG (A and C–F) of the DAG kinase inhibitor R59949 (100  $\mu$ M, B), of 100  $\mu$ M carbachol (CCh, B–E), and 300  $\mu$ M LaCl<sub>3</sub> (A and E) are indicated. (C and D) Cells were preincubated with the PKC inhibitors 1  $\mu$ M BIM I (C) or 1  $\mu$ M staurosporine (D) for 15 min. CD analysis shows summary of CDs before and during application of OAG (A and C–F), R59949 (B), CCh (B–E), or LaCl<sub>3</sub> (A and F). Numbers over bars indicate the number of measured cells and of independent transfections measured on different experimental days. (A–F) Significant differences were calculated compared with basal CDs before application of stimuli (mean  $\pm$  SEM two-tailed, paired t test; \* $P$  < 0.05, \*\* $P$  < 0.01, \*\*\* $P$  < 0.001).

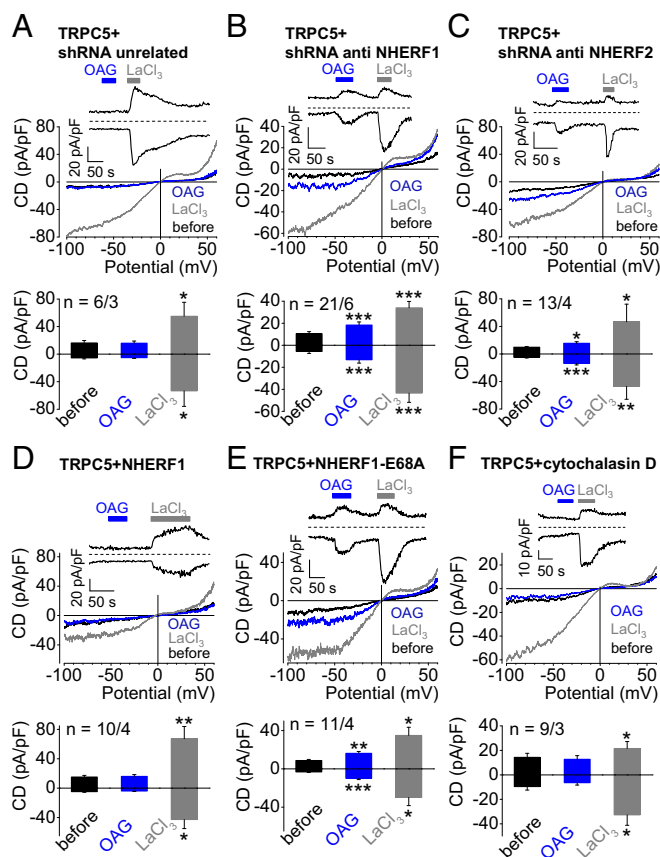


**Fig. 2.** C-terminal NHERF interaction determines OAG sensitivity of TRPC5. (A–F) Whole-cell measurements of HEK293 cells coexpressing TRPC5 together with unrelated control shRNA (A), shRNA directed against NHERF1 (B), shRNA directed against NHERF2 (C), NHERF1 (D), or the patient mutant NHERF1–E68A (E) or of HEK293 cells expressing TRPC5 channels alone (F). (F) Cells were preincubated with 5  $\mu$ M cytochalasin D for 30 min. Representative CD voltage curves and summaries of current densities at holding potentials of  $\pm 60$  mV are shown. CD analysis shows summary of CDs before and during application of 100  $\mu$ M OAG and 300  $\mu$ M LaCl<sub>3</sub>. Numbers over bars indicate the number of measured cells and of independent transfections measured on different experimental days. Significant differences compared with basal CDs before application of stimuli (mean  $\pm$  SEM, two-tailed, paired *t* test; \**P* < 0.05, \*\**P* < 0.01, \*\*\**P* < 0.001).

direct interaction of NHERF proteins with TRPC4/5 channels rather than interaction with the cytoskeleton via ERM proteins determines the DAG sensitivity of TRPC5 channels, we incubated TRPC5-expressing HEK293 cells with 5  $\mu$ M cytochalasin D, an inhibitor of actin polymerization, for 30 min to disrupt the actin cytoskeleton. Cytochalasin D-treated cells were not sensitive to OAG (Fig. 2F), whereas PKC inhibition with BIM I resulted in OAG sensitivity of cytochalasin D-treated cells (SI Appendix, Fig. S4C) similar to untreated cells. These findings indicate that NHERF binding to the actin cytoskeleton is not required for TRPC4/5 to become DAG sensitive. Altogether, these findings are in line with the concept that dissociation of NHERF1 and -2 from the C terminus of TRPC5 imparts OAG sensitivity to TRPC5.

**Coexpression of G<sub>q/11</sub>-Coupled Receptors Causes OAG Sensitivity Due to Dissociation of NHERF1 from the C Terminus of TRPC5.** Unexpectedly, OAG significantly increased TRPC5 currents in HEK293 cells coexpressing TRPC5 and G<sub>q/11</sub>-coupled receptors like muscarinic M<sub>5</sub> (M<sub>5</sub>R, Fig. 3A) or histamine H<sub>1</sub> receptors (H<sub>1</sub>Rs, SI Appendix, Fig. S5A). Endogenous DAG accumulation by application of the DAG lipase inhibitors RHC-80267 (Fig. 3B) and

orlistat (SI Appendix, Fig. S5B) or by the DAG kinase inhibitor R59949 (SI Appendix, Fig. S5C) likewise caused TRPC5 channel activation. These findings were corroborated by performing single-channel measurements in the outside-out configuration. Whereas TRPC5-expressing cells were not sensitive to OAG (SI Appendix, Fig. S6), M<sub>5</sub>R-coexpressing cells showed markedly increased single-channel activity upon OAG application at a holding potential of  $-60$  mV displayed as increases in channel open probability (NPo) (Fig. 3C). The single-channel amplitude was  $\sim 2.2$  pA reflecting a single-channel conductance of 38 pS at  $-60$  mV as estimated for TRPC5 currents (36). Additional pretreatment of TRPC5 and receptor-expressing cells with the PKC inhibitors staurosporine and BIM I and with phorbol 12,13-didecanoate (PDD), resulting in PKC down-regulation after 48 h had no effect on OAG-induced TRPC5 currents (SI Appendix, Fig. S7). Moreover, we performed whole-cell measurements with HEK293 cells transiently transfected with the most abundantly expressed isoforms TRPC4 $\alpha$  and TRPC4 $\beta$ . As a positive control, the potent TRPC4/5 channel activator englerin A (50 nM) (37) was applied and caused maximal current increases. TRPC4 $\alpha$  or TRPC4 $\beta$  channel-expressing cells were not DAG sensitive (SI Appendix, Fig. S8 A and B), whereas overexpression of GPCRs conferred DAG sensitivity to the channels (SI Appendix, Fig. S8 C and D). TRPC4 channels are activated via both G<sub>q/11</sub> and the G<sub>i/o</sub> signaling pathways. To elicit robust TRPC4 currents by agonist stimulation, we coexpressed G<sub>q/11</sub>-coupled histamine H<sub>1</sub> receptors with G<sub>i/o</sub>-coupled adrenergic  $\alpha_{2A}$  receptors. Application of an agonist mixture of 100  $\mu$ M histamine and 100  $\mu$ M noradrenaline significantly increased TRPC4 currents. TRPC4 channels became OAG sensitive in the presence of overexpressed GPCRs similar to TRPC5 channels. Moreover, PKC inhibition with BIM I (SI Appendix, Fig. S8E) and PIP<sub>2</sub> depletion using wortmannin caused OAG sensitivity of TRPC4 $\beta$ -expressing cells (SI Appendix, Fig. S8F), suggesting that TRPC4 and TRPC5 channels are regulated in a similar manner. These conclusions were supported by calcium and manganese influx experiments in fura-2-loaded HEK293 cells (SI Appendix, Fig. S9). To understand the effect of receptor coexpression in more detail, we first asked whether receptor overexpression might cause down-regulation of PKC. However, we did not note any differences in PKC levels of TRPC5 and/or receptor coexpressing cells in the presence or absence of carbachol (Fig. 3D), whereas incubation with the PKC inhibitor PDD for 48 h significantly reduced PKC protein levels. To investigate whether NHERF interaction might be involved, we performed coimmunoprecipitations with CHO-K1 cells stably expressing NHERF1. Cells were transfected with plasmids coding for HA-tagged TRPC5 and M<sub>5</sub>R (Fig. 3E). The interaction of TRPC5 and NHERF1 was confirmed by Western analysis. However, in TRPC5-, M<sub>5</sub>R-, and NHERF1-coexpressing cells, the interaction of TRPC5 and NHERF1 was lost. These findings are compatible with the notion that receptor overexpression entails separation of NHERF1 from TRPC5, thereby conferring DAG sensitivity on the channel.

**Endogenously Expressed TRPC4 and -5 Channels Become OAG Sensitive, if PKC and NHERF Interaction Are Inhibited.** To investigate whether endogenous TRPC4 and -5 channels are DAG sensitive as well, we first analyzed HKC8 cells, a human renal proximal tubule cell line (38) endogenously expressing high TRPC4 levels (39). These cells display several characteristics of proximal tubule cells like polarization, sodium-dependent uptake of phosphate, and responsiveness to parathyroid hormone (PTH). Moreover, in proximal tubule cells inappropriate renal phosphate reabsorption in patients carrying the NHERF1–E68A mutation was observed (35). By qRT-PCR, we found that proximal tubule cell markers like type II sodium-dependent phosphate cotransporter (NPT2), aminopeptidase N (ANPEP) and PTH<sub>1</sub> receptor (PTH<sub>1</sub>R) as well as NHERF1 and -2 are expressed in HKC8 cells (Fig. 4A). NHERF1 mRNA expression was nearly 40-fold higher compared with NHERF2 expression. Furthermore, TRPC1, -3, -4, -5, and -7, but not

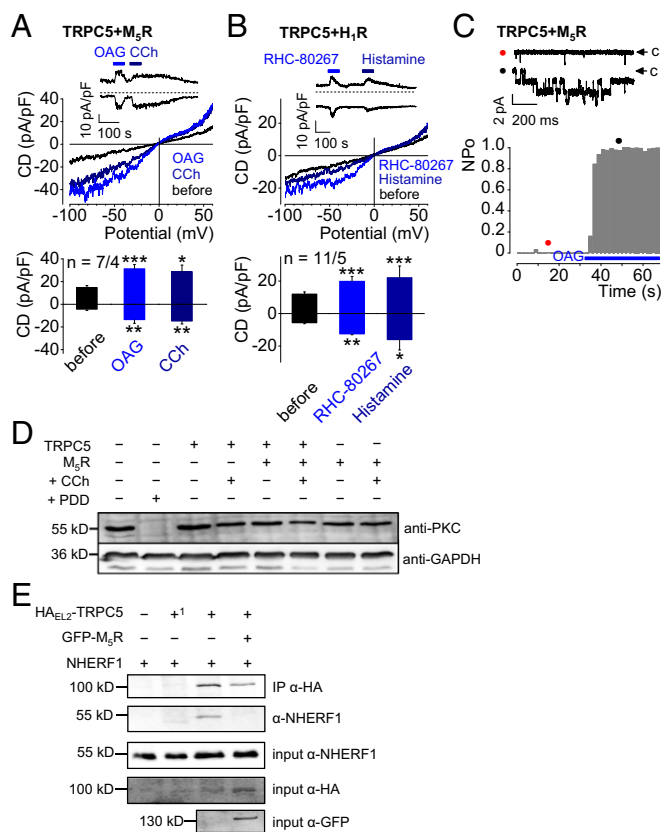


**Fig. 3.** Coexpression of  $G_{q/11}$ -coupled receptors causes OAG sensitivity due to dissociation of NHERF1 from the C terminus of TRPC5. (A and B) Whole-cell recordings of HEK293 cells coexpressing TRPC5 and  $M_5R$  (A) or TRPC5 and  $H_1R$  (B) with representative CD voltage curves, CD time courses, and summary of CDs at holding potentials of  $\pm 60$  mV. CD analysis shows summary of CDs before and during application of 100  $\mu$ M OAG (A), of the DAG lipase inhibitor RHC-80267 (100  $\mu$ M) (B), 100  $\mu$ M carbachol (CCh) (A), and 100  $\mu$ M histamine (B). Numbers over bars indicate the number of measured cells and of independent transfections measured on different experimental days. Stippled lines indicate zero currents. Applications of OAG and CCh (A) and RHC-80267 and histamine (B) are indicated. (A and B) Significant differences were calculated compared with basal CDs before application of stimuli (mean  $\pm$  SEM, two-tailed, paired  $t$  test; \* $P$  < 0.05, \*\* $P$  < 0.01, \*\*\* $P$  < 0.001). (C) Single-channel measurement in the outside-out configuration of TRPC5- and  $M_5R$ -expressing HEK293 cells. Representative current time course at  $-60$  mV before (Top, red dot) and during OAG application (Bottom, black dot) at indicated time points (red and black dots). (Bottom) Analysis of NPo before and during OAG application. C indicates the closed channel state. (D) Representative Western blot analysis of PKC levels in HEK293 cells expressing TRPC5 and/or  $M_5R$  with or without preincubation with CCh for 30 min or after incubation with 2  $\mu$ M PDD for 48 h. (E) Representative coimmunoprecipitation of TRPC5, which was HA tagged in the second extracellular loop (HA<sub>EL2</sub>-TRPC5) or of N-terminally GFP-tagged  $M_5R$  (GFP- $M_5R$ ) with coexpressed human NHERF1 in CHO-K1 cells. Immunoprecipitation with anti-HA antibody and Western blot with anti-NHERF antibody after immunoprecipitation (Upper). Coimmunoprecipitation was only observed with TRPC5 and NHERF1 coexpressing cells. Superscript 1 indicates that cell lysate was incubated with control antibody instead of anti-HA antibody. No interaction was found after incubation with control antibody. (Lower) Western blots of total cell lysates using the indicated antibodies, which served as input controls.

TRPC6 mRNA was expressed. Highest TRPC mRNA expression levels were observed for TRPC1 and TRPC4. TRPC3 mRNA expression was 5.6-fold and TRPC7 expression was 8.9-fold lower than TRPC4 expression. By patch-clamp whole-cell measurements with HKC8 cells, we found that HKC8 cells were not OAG sensitive and only  $La^{3+}$  caused significant cation current increases (Fig. 4B). Thus, in accord with our observations with recombinant proteins, endogenous TRPC4 channels are not OAG sensitive.

However, PKC inhibition with BIM I (Fig. 4C and D) and coexpression of NHERF1-E68A (Fig. 4E) rendered HKC8 cells responsive to OAG. The TRPC4 channel blocker ML 204 (40, 41) (20  $\mu$ M) prevented increases of OAG-induced TRPC4 currents after PKC inhibition (Fig. 4D). These findings suggest that in HKC8 cells, OAG induces TRPC4 currents, but not those of the sparsely expressed TRPC3/7 channels.

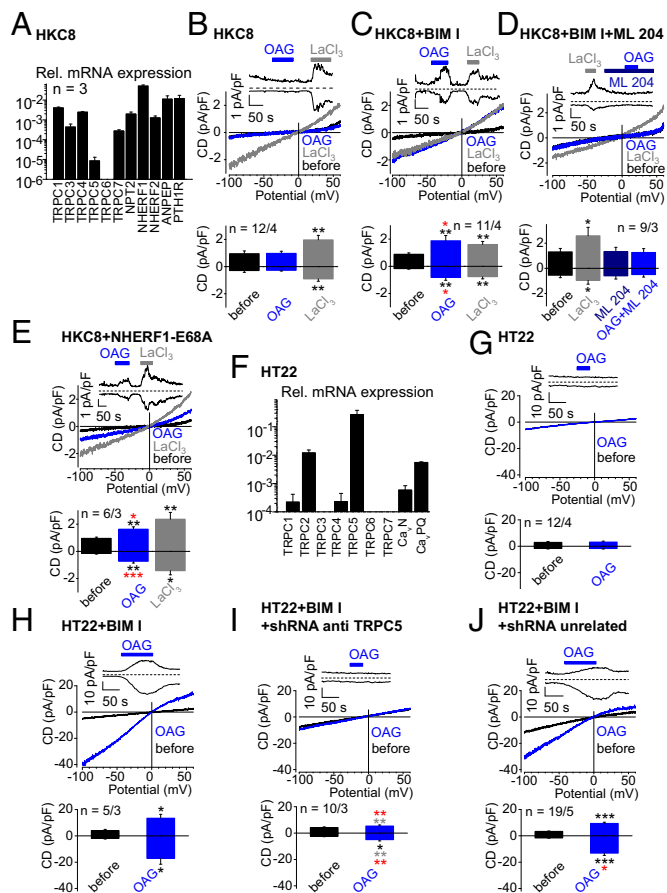


**Fig. 4.** Endogenously expressed TRPC4 and -5 channels become OAG sensitive if PKC and NHERF interaction is inhibited. (A) Summary of qRT-PCR of HKC8 cells of three independent experiments. (B–E) Whole-cell measurements of HKC8 cells without (B) or with preincubation of 1  $\mu$ M BIM I for 15 min (C and D) and after transfection with NHERF-E68A (E). (D) Application of the TRPC4 blocker ML 204 (20  $\mu$ M) is indicated. (A–E) Representative CD voltage curves, CD time courses, and summaries of CDs at holding potentials of  $\pm 60$  mV are shown. CD analysis shows summary of CDs before and during application of 100  $\mu$ M OAG in the presence (A, C, and E) or absence (D) of ML 204 and of 300 nM  $LaCl_3$ . Numbers over bars indicate the number of measured cells and independent experimental days. Significant differences compared with basal CDs (mean  $\pm$  SEM, two-tailed, paired  $t$  test; \* $P$  < 0.05, \*\* $P$  < 0.01, \*\*\* $P$  < 0.001, black asterisks) and compared with untreated HKC8 cells (mean  $\pm$  SEM, two-tailed, unpaired  $t$  test; \* $P$  < 0.05, \*\* $P$  < 0.01, \*\*\* $P$  < 0.001, red asterisks). (F) Summary of qRT-PCR of HT22 cells of three independent experiments. (G–J) Whole-cell measurements of HT22 cells without (G) or with preincubation of 1  $\mu$ M BIM I for 15 min (H). (I and J) HT22 cells transfected with shRNA directed against TRPC5 (I) or with unrelated control shRNA (J) incubated with BIM I. Representative CD voltage curves, CD time courses, and summaries of CDs at holding potentials of  $\pm 60$  mV are shown. CD analysis shows summary of CDs before and during application of 100  $\mu$ M OAG. Numbers over bars indicate the number of measured cells and independent experiments. Significant differences compared with basal CDs (mean  $\pm$  SEM, two-tailed, paired  $t$  test; \* $P$  < 0.05, \*\*\* $P$  < 0.001, black asterisks), compared with untransfected and BIM I-treated HKC8 cells (mean  $\pm$  SEM, two-tailed, unpaired  $t$  test; \* $P$  < 0.05, \*\* $P$  < 0.01, \*\*\* $P$  < 0.001, red asterisks) and compared with BIM I-treated cells expressing unrelated shRNA (mean  $\pm$  SEM, two-tailed, unpaired  $t$  test; \*\* $P$  < 0.01, gray asterisks).

Because TRPC5 channels are known to be highly expressed in the hippocampus, we next analyzed the hippocampal neuronal cell line HT22, which is commonly used as a model for glutamate-induced toxicity (42). These cells express high levels of TRPC5 mRNA, but no message of TRPC3, -6, and -7 (Fig. 4F). TRPC1, -2, and -4 were expressed less abundantly and voltage-gated calcium channels of the N- and P/Q-type were also detectable. Similar to HKC8 cells, HT22 neurons were not OAG sensitive (Fig. 4G). However, PKC inhibition by BIM I elicited OAG-induced cation currents (Fig. 4H) that were significantly suppressed by shRNA directed against TRPC5 (Fig. 4I), but not by unrelated shRNA (Fig. 4J). Altogether, these findings indicate that with regard to OAG sensitivity, endogenous TRPC4 and -5 mirror functional characteristics of heterologously expressed ion channels.

**PIP<sub>2</sub> Depletion Renders TRPC5 Channels DAG Sensitive.** In contrast to other TRPC channels, TRPC4 and -5 are inhibited by PIP<sub>2</sub> and depletion of the phospholipid results in current potentiation (11, 12, 43). It has been postulated that membrane-bound PIP<sub>2</sub> interacts with the C terminus of TRPC4 $\alpha$ , thereby stabilizing the closed channel conformation in the presence of NHERF1 (11). To investigate whether PIP<sub>2</sub> depletion contributes to DAG sensitivity, we performed whole-cell patch-clamp measurements with TRPC5-expressing HEK293 cells and depleted PIP<sub>2</sub> by several different maneuvers. Wortmannin, a phosphoinositide 3-kinase inhibitor at low (<100 nM) and a phosphoinositide 4-kinase inhibitor at high concentrations (20  $\mu$ M), were administered. A total of 20  $\mu$ M wortmannin increased TRPC5 currents that were further enhanced by additional application of OAG (Fig. 5A). As a control, wortmannin was also applied at low concentrations (100 nM). Application of 100 nM wortmannin and additional application of OAG had no effect (Fig. 5B), indicating that OAG sensitivity of TRPC5 is independent of phosphoinositide 3-kinase inhibition. Similar results were obtained by application of LY294002, a more potent inhibitor of phosphoinositide 4-kinases at higher concentrations (100  $\mu$ M) (Fig. 5C) and of poly-L-lysine (PLL) (3  $\mu$ g/mL), a scavenger of PIP<sub>2</sub>, applied through the patch pipette (Fig. 5D), both leading to OAG sensitivity. Furthermore, PIP<sub>2</sub> depletion was induced by coexpressing the membrane-associated rapamycin-binding protein Lyn11-FRB-mCherry together with the cytosolic and also rapamycin-binding protein pseudojanin-FKBP-pmRFP-C1, which is fused to the two phosphatases Sac1 and INPP5E. Application of rapamycin causes translocation of pseudojanin-FKBP-pmRFP-C1 to the cell membrane, leading to rapamycin-induced degradation of PIP<sub>2</sub> to PI(4)P and to phosphatidylinositol (PI) (44) (Fig. 5E). In all experimental conditions tested, PIP<sub>2</sub> depletion resulted in OAG sensitivity of TRPC5. Interestingly, PIP<sub>2</sub> depletion caused current increases of 38% at -60 mV compared with maximal OAG-induced currents (100%). Moreover, TRPC5-T972E mutant channels became OAG sensitive upon application of wortmannin similar to wild-type TRPC5 channels (SI Appendix, Fig. S4D). Because G<sub>q/11</sub>-coupled receptor stimulation leads to PLC-dependent PIP<sub>2</sub> degradation as well, we next analyzed whether TRPC5 channels might likewise become OAG sensitive during receptor activation. To this end, perforated-patch measurements were performed that leave the endogenous calcium buffering unaffected. Carbachol-induced activation of endogenous muscarinic M<sub>3</sub> receptors caused small but significant TRPC5 current increases of 36% of OAG-induced maximal currents in TRPC5 expressing HEK293 cells at -60 mV (Fig. 5F), similar to the currents induced by PIP<sub>2</sub> depletion. These findings lend further support to the notion that PIP<sub>2</sub> depletion results in OAG sensitivity of TRPC5 and that PIP<sub>2</sub> depletion stabilizes an active channel conformation, allowing for current increases of ~40%.

**PIP<sub>2</sub> Depletion and G<sub>q/11</sub>-Coupled Receptor Activation Lead to Dynamic NHERF1 Dissociation and a Conformational Change of the TRPC5 C Terminus.** The finding that PIP<sub>2</sub> degradation with or without involvement of PLC entails OAG sensitivity of TRPC5 raised the

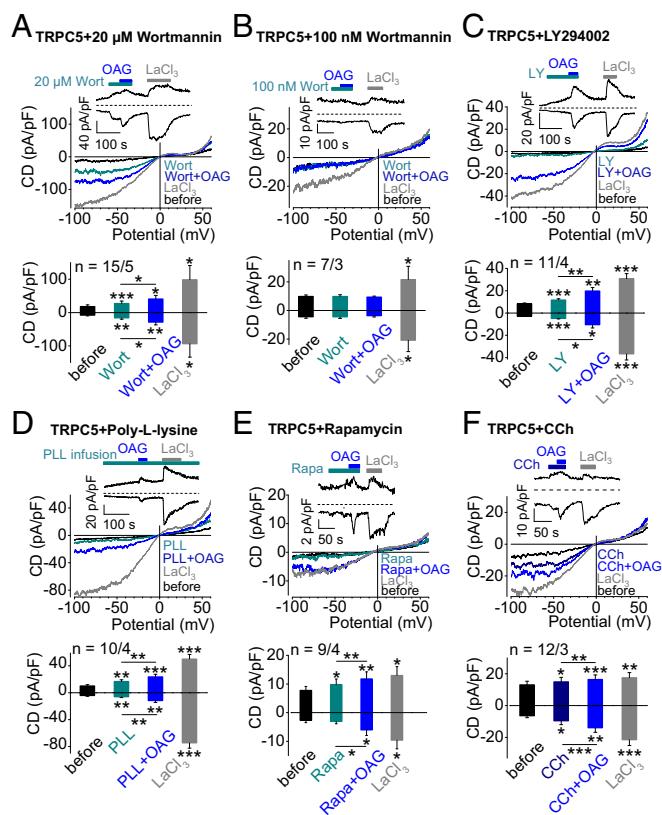


**Fig. 5.** PIP<sub>2</sub> depletion renders TRPC5 channels DAG sensitive. (A–F) Whole-cell measurements of HEK293 cells expressing TRPC5 alone (A–D and E) or together with Lyn11-FRB-mCherry and pseudojanin-FKBP-pmRFP-C1, which is fused to the phosphatases Sac1 and INPP5E leading to rapamycin-induced degradation of PIP<sub>2</sub> to PI(4)P and to PI (E). Representative CD voltage curves, CD time courses, and summaries of CDs at holding potentials of  $\pm 60$  mV are shown. CD analysis shows summary of CDs before and during application of 100  $\mu$ M OAG in the presence of 20  $\mu$ M wortmannin (A), 100 nM wortmannin (B), 100  $\mu$ M LY294002 (C), 3  $\mu$ g/mL poly-L-lysine (PLL) (D), 5  $\mu$ M rapamycin (E), 100  $\mu$ M carbachol (CCh) (F), and during application of 300  $\mu$ M LaCl<sub>3</sub>. Numbers over bars indicate the number of measured cells and independent experiments measured at different experimental days. Bath applications of OAG, LaCl<sub>3</sub>, and of wortmannin (A and B), LY294002 (C), rapamycin (E), and CCh (F) are indicated. PLL was applied through the patch pipette (D). Stippled line indicates zero current. Significant differences are compared with basal CDs (mean  $\pm$  SEM, two-tailed, paired *t* test; \*\**P* < 0.01, \**P* < 0.05, \*\*\**P* < 0.001). Significant differences between CDs induced by PIP<sub>2</sub> depletions with wortmannin, LY294002, PLL, rapamycin, or CCh compared with additional application of OAG (mean  $\pm$  SEM, two-tailed, paired *t* test; \**P* < 0.05, \*\**P* < 0.01, \*\*\**P* < 0.001).

question of whether OAG sensitivity might be due to dissociation of NHERF1 and -2 proteins. To shed further light on the molecular mechanisms involved, the technique of dynamic intermolecular fluorescence resonance energy transfer (FRET) was used, drawing on HEK293 cells stably expressing N-terminally Cerulean (a stable cyan fluorescent protein)-tagged NHERF1 serving as a FRET donor, and transiently expressing C-terminally eYFP-tagged TRPC5 representing a FRET acceptor. PIP<sub>2</sub> depletion by wortmannin (20  $\mu$ M) resulted in increased Cerulean and decreased eYFP fluorescence, thus leading to decreased FRET signals (Fig. 6A), suggestive of an increased distance between the two fluorophores. Receptor stimulation with carbachol had a similar effect. Thus, PIP<sub>2</sub> degradation by whatever means results in the dissociation of NHERF1 from the C terminus of TRPC5. The pseudophosphorylated TRPC5-T972D mutant behaved similarly to wild-type TRPC5 (Fig. 6B), although the amplitudes of the FRET signals were less pronounced consistent with the concept that phosphorylation of

T972 increases the affinity of NHERF1 to the C terminus of TRPC5. In addition, the nonphosphorylatable TRPC5–T972A mutant showed no response to wortmannin or carbachol applications (Fig. 6C), indicating that phosphorylation at position T972 is essential for NHERF1 binding. Additionally, TRPC6 unable to interact with NHERF1 was used as a negative control (Fig. 6D). The summary of the wortmannin- and carbachol-induced FRET signal changes illustrates that only wild-type TRPC5 and the TRPC5–T972D mutant, but not TRPC5–T972A- or TRPC6-expressing cells, displayed dynamic NHERF1 interactions (Fig. 6E).

To investigate whether NHERF1 dissociation is accompanied by a conformational change of the TRPC5 C terminus, we performed FRET experiments with HEK293 cells coexpressing TRPC5 proteins, which were C-terminally fused either to eCFP serving as a FRET donor or to eYFP as a FRET acceptor. PIP<sub>2</sub> depletion with wortmannin increased FRET signals, indicating that in tetrameric TRPC5 channel complexes, C termini come into close vicinity (Fig. 6F). However, whereas OAG alone had no effect (Fig. 6G), OAG application in the presence of wortmannin caused even higher FRET signals (Fig. 6H). In addition, activation of endogenous G<sub>q/11</sub>-coupled P2Y receptors in HEK293 cells by 100 μM ATP also increased FRET signals similar to wortmannin application (Fig. 6I). These findings are concordant with the notion that PIP<sub>2</sub> depletion causes a conformational change of the C terminus. This DAG-sensitive channel conformation is reflected by current increases of about 40% induced by PIP<sub>2</sub> depletions (Fig. 5 A–D). Further increases in FRET signals engendered by additional OAG application probably are the conformational equivalent of OAG-induced maximal currents. Altogether, OAG-induced TRPC5 channel activation is accompanied by a rearrangement of the C termini of TRPC5 proteins. As a control, the TRPC5–T972A mutant C-terminally fused to eCFP or eYFP was analyzed. PIP<sub>2</sub> depletion caused FRET signal increases similar to wild-type channels (Fig. 6J), suggesting a C-terminal conformational change. In contrast to wild-type channels, however, OAG stimulation alone also entailed an increase in FRET signals (Fig. 6K). Moreover, OAG further enhanced FRET signals in the presence of wortmannin (Fig. 6L). Application of ATP also increased FRET signals similar to wild-type TRPC5 channels (Fig. 6M). The summaries of the FRET signal alterations show that OAG has no effect on wild-type TRPC5, but on TRPC5–T972A channels, and PIP<sub>2</sub> depletion with or without involvement of PLC engages an OAG-sensitive channel conformation accompanied by a rearrangement of TRPC5 C-termini (Fig. 6N). In conclusion, PIP<sub>2</sub> depletion and G<sub>q/11</sub>-coupled receptor activation cause a C-terminal movement and concurrent dislocation of NHERF, thereby inducing a DAG-sensitive channel state.

## Discussion

Until now, the activation mechanism of TRPC4 and -5 channels subsequent to engagement of G<sub>q/11</sub>-coupled receptors has remained largely elusive, because, in contrast to all other TRPC channels (7–9), the PLC product DAG is not sufficient for channel activation (8). Interestingly, TRPC4/5 channels are not only activated via the G<sub>q/11</sub>-protein–PLC pathway, but probably also subsequent to G<sub>i/o</sub>-coupled receptor activation (45, 46). However, the mechanisms of G<sub>i/o</sub>-mediated TRPC4/5 activation are still not completely understood and might involve either direct G<sub>i/o</sub> protein interaction (45) or activation of PLCδ1 (46). It was speculated that PLC-mediated PIP<sub>2</sub> depletion might be involved in TRPC4 and -5 channel activation (11, 12), even though there was initial evidence that TRPC5 channels might be DAG sensitive as well (10, 14). In contrast to other TRPC channels, TRPC4 and -5 channels possess a C-terminal PDZ-binding motif, allowing for interaction with the adaptor proteins NHERF1 and -2. The specific role of this protein interaction for TRPC4 and -5 channel function, however, has not been sorted out so far. In this

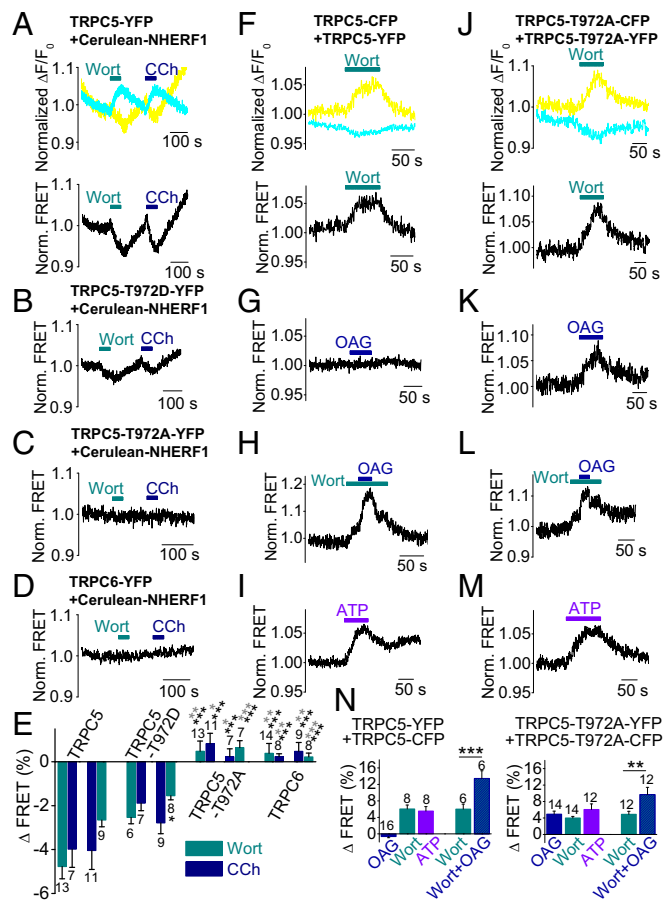


**Fig. 6.** PIP<sub>2</sub> depletion and G<sub>q/11</sub>-coupled receptor activation lead to dynamic NHERF1 dissociation and a conformational change of the TRPC5 C terminus. (A–M) Dynamic intermolecular FRET measurements with dual-emission photometry. (A–E) FRET measurements between N-terminally Cerulean-tagged NHERF1 (Cerulean–NHERF1) and (A) C-terminally eYFP-tagged TRPC5 (TRPC5–YFP), (B) C-terminally eYFP-tagged TRPC5–T972D (TRPC5–T972D–YFP), (C) C-terminally eYFP-tagged TRPC5–T972A (TRPC5–T972A–YFP), and (D) C-terminally eYFP-tagged TRPC6 (TRPC6–YFP). (A) Representative FRET measurement showing normalized fluorescence traces of Cerulean (cyan) and eYFP (yellow) on excitation of 430 nm (Left). (A–D) Representative traces of the FRET signal. Applications of 20 μM wortmannin (Wort) and of 100 μM carbachol (CCh) are indicated. (E) Summary of changes of FRET signal amplitudes induced by wortmannin (cyan bars) or CCh (dark blue bars) in both orders of application. Numbers indicate the numbers of measured cells from at least four independent experiments. Significant differences compared with wild-type TRPC5–eYFP-expressing cells (mean ± SEM, two-tailed, unpaired t test; \*\**P* < 0.01, \*\*\**P* < 0.001, black asterisks). Significant differences compared with TRPC5–T972D–eYFP-expressing cells (mean ± SEM, two-tailed, unpaired t test; \*\**P* < 0.01, \*\*\**P* < 0.001, gray asterisk). (F–N) FRET measurements between C-terminally eYFP- and eCFP-tagged TRPC5 (F–I) and between C-terminally eYFP- and eCFP-tagged TRPC5–T972A (J–M). (F and J) Representative FRET measurement showing normalized fluorescence traces of eCFP (cyan) and eYFP (yellow) on excitation of 430 nm (Left). (F–M) Representative traces of the FRET signal. Applications of 20 μM wortmannin (Wort), of 100 μM ATP, and of 100 μM OAG are indicated. (N) Summaries of changes of FRET signal amplitudes induced by wortmannin (cyan bars), ATP (violet bars), OAG (blue bars), and OAG and wortmannin together (blue hatched bars). Numbers indicate the numbers of measured cells from at least four independent experiments. Significant differences between wortmannin- and wortmannin plus OAG-induced FRET amplitudes (mean ± SEM, two-tailed, unpaired t test; \*\**P* < 0.01, \*\*\**P* < 0.001, black asterisks).

study, we demonstrate that TRPC4 and -5 become sensitive to DAG if the NHERF adaptor proteins dissociate from the C terminus. Taking into account that C-terminal phosphorylation by

PKC is required for TRPC4/5–NHERF interaction, DAG sensitivity is achieved under the following experimental paradigms: (i) PKC inhibition, (ii) removal of a C-terminal PKC phosphorylation site in the PDZ-binding motif, (iii) NHERF1 and -2 down-regulation, (iv) coexpression of a NHERF1 mutant (NHERF1–E68A) incapable of C-terminal TRPC5 interaction, (v) coexpression of  $G_{q/11}$ -coupled receptors, and (vi) C-terminal conformational rearrangements engendered by  $PIP_2$  depletion. Our findings based on electrophysiology, coimmunoprecipitations, and intermolecular FRET suggest that a crucial step in TRPC5 activation is the dissociation of NHERF proteins from the channel C terminus, thus conferring DAG sensitivity. NHERF binding was previously described to enhance trafficking of the inwardly rectifying potassium channel Kir 1.1 and acid-sensing ion channel 3 (47, 48), to stabilize TRPV5 at the plasma membrane (49), and to increase gating of cystic fibrosis transmembrane conductance regulator channels (50). Our findings define an unexpected functional role of NHERF proteins as critical dynamic regulators of TRPC5 channel activity.

Our findings support a paradigm with the potential to combine different discrepant findings on  $G_{q/11}$  protein-mediated TRPC5 channel activation in a unifying model: C-terminal NHERF and  $PIP_2$  interaction stabilize a DAG-insensitive, -inactive channel conformation. During receptor activation,  $PIP_2$  at the plasma membrane is degraded by PLC resulting in an active TRPC5 conformation characterized by C-terminal rearrangements and the ensuing dissociation of NHERF1 and -2, thereby conferring DAG sensitivity upon TRPC4 and -5 channels (summarized and illustrated in Fig. 7). Therefore, TRPC5 has to be classified as DAG sensitive like the members of the TRPC3/6/7 subfamily. Notably,  $PIP_2$  depletion evokes only small increases in TRPC5 currents, whereas additional application of DAG results in full TRPC5 activation, indicating that  $PIP_2$  depletion is necessary, but not sufficient to fully activate TRPC5 channels.

Experiments with TRPC4 channels showed that TRPC4 is also DAG sensitive if GPCRs are coexpressed, PKC is inhibited, and  $PIP_2$  depleted. However, our findings that  $PIP_2$  depletion results in TRPC4 $\beta$  current increases and subsequently renders TRPC4 $\beta$  channels sensitive to DAG (SI Appendix, Fig. S8F) are in contrast to observations by Kim et al. (51). In the latter study,  $PIP_2$  depletion inhibited TRPC4 $\beta$  currents. Different experimental settings may have contributed to these contradictory findings. In contrast to our experiments, Kim et al. (51) preactivated TRPC4 $\beta$  channels by infusions with the nonhydrolyzable GTP analog GTP $\gamma$ S and used a nonphysiological bath solution containing high  $Cs^+$  (140 mM). The latter measure amplified TRPC4 inward and outward currents about 10-fold compared with those in physiological bath solutions. Infusion of GTP $\gamma$ S induces various G protein-dependent signal transduction pathways, including PLC-mediated  $PIP_2$  cleavage and activation of PKC leading to channel desensitization. These experimental conditions may mask the current increases we observe upon  $PIP_2$  depletion. However, our findings in the overexpression system are further supported by experiments with the proximal tubule cell line HKC8 expressing high mRNA levels of TRPC4 and NHERF1 and only marginal levels of TRPC5, but no TRPC6. Accordingly, HKC8 cells were not directly DAG sensitive. Application of 300  $\mu$ M  $La^{3+}$  increased cation currents, illustrating that TRPC4, but not TRPC3 or -7 currents were induced, because the latter channels would be inhibited by  $La^{3+}$  (34, 52–55). HKC8 cells were rendered OAG sensitive subsequent to PKC inhibition or coexpression of the NHERF1–E68A mutant harboring a disrupted PDZ1 domain impairing its interaction with TRPC4 and -5 channels. The NHERF1–E68A mutation was first identified in patients with inappropriate renal phosphate reabsorption (35). Interestingly, OAG- and  $La^{3+}$ -induced currents in HKC8 cells showed similar current–voltage relationships, suggesting that in both cases TRPC4 channels are activated. Endogenously expressed TRPC5 channels were also DAG sensitive as shown in murine hippocampal neurons (HT22 cells) (56, 57) expressing high

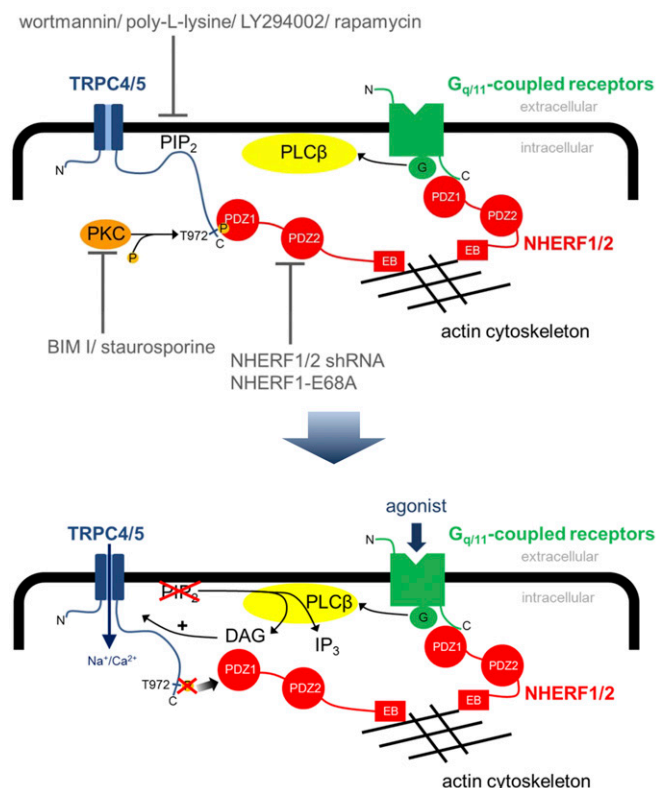


**Fig. 7.** Model of receptor-operated TRPC4 and -5 channel activation by DAG. In the DAG-insensitive, inactive channel conformation,  $PIP_2$  and NHERF proteins are bound to the C terminus.  $PIP_2$  depletion, PKC inhibition, NHERF down-regulation, and coexpression of the NHERF1–E68A mutant lead to DAG sensitivity. PLC-dependent or independent  $PIP_2$  depletions cause a conformational change of the C terminus, leading to dissociation of NHERF, which results in DAG sensitivity of TRPC4 and -5 channels.

TRPC5 mRNA levels. Thus, endogenously expressed TRPC4 and -5 channels were found to be DAG sensitive upon PKC inhibition similar to overexpressed channels.  $G_{q/11}$  protein-mediated TRPC5 activation is of physiological importance in stomach smooth muscle cells and leads to smooth muscle cell contraction (14). In pyramidal cells of the cerebral cortex  $G_{q/11}$ -dependent TRPC5 activation results in slow afterdepolarizations (58). Moreover,  $G_{q/11}$  protein-mediated TRPC4 activation regulates gonadotropin-releasing hormone (GnRH) secretion in GnRH neurons (59, 60).

NHERF1 dissociation from TRPC5 was determined by immunoprecipitations and dynamic intermolecular FRET. Unexpectedly,  $G_{q/11}$ -coupled receptor overexpression led to dissociation of NHERF1 from the C terminus of TRPC5. Because NHERF1 binding to the C terminus of several receptors such as adrenergic  $\beta_2$ ,  $PTH_1$ , and A2b receptors (summarized in ref. 61) via its PDZ1 domain is a well-described phenomenon, one may speculate that NHERF1 is scavenged by overexpressed receptors. By performing dynamic intermolecular FRET with fluorescence-tagged TRPC5 and NHERF1 constructs, we found that receptor activation and  $PIP_2$  depletion both caused dissociation of NHERF1 from the C terminus of TRPC5 in a reversible and repeatable manner. There was no significant difference between the first or the second stimulation with carbachol and wortmannin, suggesting that inactivation of the channel during the time course of the experiments was negligible. As expected, TRPC5–T972A- and TRPC6-expressing cells showed no FRET decreases upon  $PIP_2$  depletion or agonist stimulation, indicating that NHERF1 is not bound to the C terminus under these conditions and thus cannot dissociate.

These findings are consistent with the assumption of dynamic C-terminal NHERF interactions determining TRPC5 channel activation by DAG.

However, the question still remains unanswered as to how PIP<sub>2</sub> interacts with the C terminus of TRPC4 and -5 (62). Direct C-terminal PIP<sub>2</sub> interaction was demonstrated for the unique TRPC4 $\alpha$  isoform (11). Truncation of the C-terminal TTRL motif of TRPC4 $\alpha$  abolished PIP<sub>2</sub>-induced channel inhibition, entertaining the notion that binding of NHERF1 and PIP<sub>2</sub> to the C terminus stabilizes an inactive channel conformation (11). However, NHERF interaction was not linked to DAG sensitivity in the latter study.

Altogether, we define a mechanism of TRPC4 and -5 channel activation and assign an unexpected functional role to NHERF proteins as critical dynamic regulators of TRPC4/5 channel activity. NHERF dissociation from TRPC4 and -5 proteins is crucial for DAG-mediated channel activation. Thus, DAG sensitivity probably is a characteristic hallmark of all TRPC channels.

## Materials and Methods

**Cell Culture.** Human embryonic kidney (HEK293) cells (ATCC CRL-3216) were maintained in Earl's MEM (Sigma-Aldrich), CHO-K1 cells were cultured in Ham's F-12 medium (Sigma-Aldrich), and HT22 cells were maintained in DMEM (Sigma-Aldrich) with 100 units/mL penicillin and 100  $\mu$ g/mL streptomycin supplemented with 10% (vol/vol) FCS (Gibco) and 2 mM glutamine. HKC8 cells, a human-derived renal proximal tubule cell line (38), were cultured in DMEM/Ham's F-12 medium 1:1 mixture supplemented with 2.5% FCS, insulin-transferrin-selenium supplement (Gibco), and 2 mM glutamine. All cells were held at 37 °C in a humidified atmosphere with 5% CO<sub>2</sub>. CHO-K1 cells stably expressing human NHERF1 [SLC9A3R1 [solute carrier family 9, subfamily A (NHE3, cation proton antiporter 3), member 3 regulator 1], NG\_013022] were cultured in Ham's F-12 medium additionally containing 800  $\mu$ g·ml<sup>-1</sup> G418 (Invitrogen).

**Materials.** Poly-L-lysine (molecular weight 4.000–15.000), 5-nitro-2-(3-phenylpropylamino)benzoic acid (NPPB), LaCl<sub>3</sub>, 4,4'-diisothiocyanostilbene-2,2'-disulfonic acid (DIDS), carbachol, histamine, phorbol 12,13-didecanoate (PDD), and wortmannin were purchased from Sigma-Aldrich. OAG, RHC-80267, R59949, BIM 1, H98, and staurosporine were from Calbiochem. Rapamycin was purchased from Cayman Chemical, LY294002 from Tocris, Englerin A from Carl Roth, and ML 204 from Tocris.

**Mutagenesis.** Amino acid exchanges from threonine to alanine, glutamate, or aspartate at position 972 in murine TRPC5 (NM\_009428) and from glutamate to alanine at position 68 in human NHERF1 (NG\_013022) were introduced by site-directed mutagenesis using the QuikChange system (Stratagene). All cDNA constructs used in the present work were confirmed by sequencing.

**Generation of shRNA.** To investigate the role of NHERF1 and NHERF2 in HEK293 cells, RNA interference was used. For this, shRNA was transiently expressed via a pSuper NeoGFP expression vector. shRNA targeting human NHERF1 and human NHERF2 was designed according to ref. 63. As a control, unrelated shRNA was expressed. The DNA sequence was 5'-GGA AAC TGA CGA GTT CTT CAA GAA ATG CA-3' for the NHERF1-specific construct, 5'-AAC AGG AAG CGT GAA ATC TTC AGC AAC TT-3' for the NHERF2-specific construct, and 5'-TTT GAT TTG CGA AGG TTT T-3' for the unrelated construct. For analysis of endogenously expressed TRPC5 in HT22 cells, shRNA targeting TRPC5 was used. The DNA sequence was 5'-ATC AAA TAT CAC CAG AAA G-3' for the TRPC5-specific construct as described elsewhere (64). For transient transfections, either Genejuice (Merck Millipore) or the NEON device (Invitrogen) were used according to the manufacturer's protocol. The efficiency of the shRNA constructs was tested using qPCR and Western blot analysis.

**qPCR Analysis.** Total RNA from HEK293, HKC8, and HT22 cells was isolated using TRI Reagent (Sigma-Aldrich). First-strand synthesis was carried out with random hexamers as primers, using REVERTAID reverse transcriptase (Fermentas). The following primer pairs for analysis of HEK293 and HKC8 cells were used for the amplification of specific fragments from the first-strand synthesis: TRPC1, C1 forward (5'-ATG GCG CTGA AGG ATGT G-3') and C1 reverse (5'-TCC TCC AAA ATC TTT TTA ACC ATA TAA-3'); TRPC3, C3 forward (5'-CAA AGA AAA TGA AGT TAA TGA AGG-3') and C3 reverse (5'-CTT GGC TCT TGT CTT CCA AAA-3'); TRPC4, C4 forward (5'-GGT CAG ACT TGA ACA GGC AAG-3') and C4 reverse (5'-GTT TAA TTT CTC CCC ATA TGA AGC-3'); human TRPC5, C5 forward (5'-GCC TGA TAC AAA ATC AAC ATT ATC A-3')

and C5 reverse (5'-CCT CAT GTG TTT TGG AAT TTC TT-3'); TRPC6, C6 forward (5'-ATT TAC TGG TTT GCT CCA TGC-3'), C6 reverse (5'-GCA GTC CCA GAA AAA TGG TG-3'); TRPC7, C7 forward (5'-GAG CGG TAC ATC CTT GGC TA-3') and C7 reverse (5'-TTT GAA GGT GCT GTT CCT CA-3'); NHERF1, NHERF1 forward (5'-GGC TGG CAA CGA AAA TGA-3') and NHERF1 reverse (5'-TTG GAC TTG TCG CTG TGC-3'); NHERF2, NHERF2 forward (5'-CGA AGC TGG CAA GAA GGA T-3') and NHERF2 reverse (5'-GAG GTC CCT TTC GCA GGT-3'); NPT2 phosphate transporter, NPT2 forward (5'-TCC AGA AGG TCA TCA ATA CGG-3') and NPT2 reverse (5'-GAC CAC GAA GGT CAT GCT G-3'); amonipeptidase N (ANPEP), ANPEP forward (5'-CAT CCA TCA GAG ATG GCA GAC-3') and ANPEP reverse (5'-TGC TGA AGA GAT CGT TCT GG-3'); PTH<sub>1</sub>R, PTH1 forward (5'-GGG GCT TCA CAG TCT TCG-3') and PTH1 reverse (5'-TGG CCA GGG TAG CTC TGA-3'); and three references hypoxanthin phosphoribosyltransferase 1, Hprt1 forward (5'-TGA CCT TGA TTT ATT TTG CAT ACC-3') and Hprt1 reverse (5'-CGA GCA AGA CGT TCA GTC CT -3'), tyrosine 3-monooxygenase/tryptophan 5-monooxygenase activation protein, zeta polypeptide, Ywhaz forward (5'-GAT CCC CAA TGC TTC ACA AG-3') and Ywhaz reverse (5'-TGC TTG TTG TGA CTG ATC GAC-3'); and succinate dehydrogenase complex, subunit A, Sdha forward (5'-GGA CCT GGT TGT CTT TGG TC-3') and Sdha reverse (5'-CCA CGC TTT GGT TTA ATT GG-3'), giving predicted product sizes of 113 bp for TRPC1, 95 bp for TRPC3, 93 bp for TRPC4, 93 bp for TRPC5, 103 bp for TRPC6, 129 bp for TRPC7, 132 bp for NHERF1, 77 bp for NHERF2, 95 bp for NPT2, 75 bp for ANPEP, 78 bp for PTH<sub>1</sub>R, 102 bp for Hprt1, 130 bp for Ywhaz, and 93 bp for Sdha. The primer pairs for analysis of murine-derived HT22 cells are described elsewhere (64). RT-PCR was performed using the master mix from the Absolute QPCR SYBR Green Mix kit (Abgene). Ten picomoles of each primer pair and 0.2  $\mu$ L of the first-strand synthesis was added to the reaction mixture, and PCR was carried out in a light-cycler apparatus (Light-Cycler 480, Roche) using the following conditions: a 15-min initial activation and 45 cycles of 12 s at 94 °C, 30 s at 50 °C, 30 s at 72 °C, and 10 s at 80 °C each. Fluorescence intensities were recorded after the extension step at 80 °C after each cycle to exclude fluorescence of primer dimers melting lower than 80 °C. All primers were tested by using diluted cDNA from the first-strand synthesis (10–1,000 times) to confirm linearity of the reaction and to determine particular efficiencies. Data were calculated as percentage of mean expression of the three references. Samples containing primer dimers were excluded by melting curve analysis and identification of the products by agarose gel electrophoresis. Crossing points were determined by the software program. All experiments were performed in quadruplets and experiments were repeated at least three times.

**SDS/PAGE and Western Blotting.** PKC and NHERF1 levels in HEK293 cells were quantified using standard SDS/PAGE and Western blot technique. For the measurement of PKC levels, cells were transiently transfected with 3  $\mu$ g mTRPC5 and 0.75  $\mu$ g rM<sub>5</sub>R (M22925.1) cDNA using lipofection. Next day, nontransfected cells were incubated with 2  $\mu$ M PDD for 24 h before isolation. Other cells were incubated with 100  $\mu$ M carbachol for 6 h before isolation. At 48 h after transfection, cells were lysed for 10 min in RIPA buffer (50 mM Tris pH 7.5, 200 mM NaCl, 1% Triton X-100, 0.25% DOC, 1 mM EDTA, 1 mM EGTA, and freshly added protease inhibitors (Fermentas)) on ice and centrifuged for half an hour at maximum speed. Supernatant was placed in SDS sample buffer and boiled for 5 min and subjected to gel electrophoresis on a 12% SDS/PAGE gel. Proteins were transferred onto PVDF membranes as described by the manufacturer (Bio-Rad). After transfer, blots were blocked with 5% milk and incubated with primary mouse PKC antibody (Sigma-Aldrich) or mouse anti-GAPDH antibody (Sigma-Aldrich) in combination with secondary anti-mouse antibody (Promega) to determine the expression of PKC and GAPDH. To confirm the efficiency of hNHERF1 and hNHERF2 shRNA, HEK293 cells were transiently transfected with hNHERF1 and hNHERF2 shRNA cDNA constructs using the NEON device (Invitrogen) as described by the manufacturer. Two days after transfection, cells were collected in RIPA buffer and processed as mentioned above. For quantification of protein levels, primary rabbit NHERF1 (Santa Cruz Biotechnology) and primary rabbit NHERF2 antibodies (Sigma-Aldrich) and secondary anti-rabbit antibody (Promega) were used. All experiments were repeated three times with comparable results.

**Coimmunoprecipitation.** For immunoprecipitation studies, a polyclonal CHO-K1 cell line stably expressing hNHERF1 was used. To allow detection of TRPC5 on Western blots, a HA tag was inserted into the second extracellular loop of mTRPC5. First, an Hpa1 restriction site was generated in mTRPC5 using site-directed mutagenesis with the following primers: mTRPC5 Hpa1 sense 5'-CGT GGC CTA TGT CAA GGT TAA CGG TTC TCG TCC A-3' and mTRPC5 Hpa1 antisense 5'-TGG ACG AGA ACC GTT AAC CTT GAC ATA GGC CAC G-3'. Mutagenesis resulted in the amino acid exchange of Tyr500 to valine. Thereafter,

construct was cut using HpaI and the HA tag was inserted using the following primers: HA-tag sense 5'-TAC CCA TAC GAT GTT CCA GAT TAC GCT-3' and HA-tag anti-sense 5'-AGC GTA ATC TGG AAC ATC GTA TGG GTA-3'. HA-EL2-mTRPC5 constructs and GFP-hM5R construct were electroporated into CHO-K1 cells stably expressing hNHERF1 using the Neon Transfection system (Life Technologies) according to the manufacturer's manual. Three days after transfection, cells were lysed using 1 mL cold RIPA lysis buffer. Subsequently, probes were frozen in liquid nitrogen to enhance lysis of cells. After thawing of probes on ice, probes were briefly shredded using the Qiagen TissueRuptor (Qiagen) to ensure better solubility of membrane bound TRPC5. Remaining debris was briefly centrifuged at full speed. A total of 150  $\mu$ L of the supernatant was taken out for input controls; the rest was used for immunoprecipitation. For immunoprecipitation, 8  $\mu$ L rat anti-HA antibody (Roche) or 8  $\mu$ L irrelevant antibody (negative control) were used. Probes were rotated overnight at 4 °C where after 80  $\mu$ L of a 50% protein A/G agarose bead slurry diluted in lysis buffer was added. Samples were rotated for 2 more hours at 4 °C, where after beads were washed five times using cold lysis buffer. Bound proteins were quantified using SDS/PAGE electrophoresis and Western blotting technique using primary rabbit NHERF1 (Santa Cruz Biotechnology) and primary anti-HA antibody (Roche).

**Electrophysiological Whole-Cell and Outside-Out Measurements.** Conventional whole-cell and outside-out patch-clamp recordings were carried out at room temperature (23 °C) 48–72 h after transfection with murine TRPC5 (NM\_009428), rat TRPC4 $\alpha$  (NM\_080396.1), or rat TRPC4 $\beta$  (AF421364.1). Cells were superfused with bath solution containing 140 mM NaCl, 5 mM CsCl, 1 mM MgCl<sub>2</sub>, 2 mM CaCl<sub>2</sub>, 10 mM glucose, 10 mM Hepes (pH 7.4 with NaOH) resulting in an osmolality of 295–302 mOsm·kg<sup>-1</sup>. HKC-8 and HT22 cells were superfused with the bath solution supplemented with the chloride channel blockers 50  $\mu$ M NPPB and 300  $\mu$ M DIDS to suppress chloride conductance. The standard pipette solution contained 120 mM CsCl, 9.4 mM NaCl, 0.2 mM Na<sub>3</sub>GTP, 1 mM MgCl<sub>2</sub>, 3.949 mM CaCl<sub>2</sub>, 10 mM BAPTA (100 nM free Ca<sup>2+</sup>), and 10 mM Hepes (pH 7.2 with CsOH), resulting in an osmolality of 294 mOsm·kg<sup>-1</sup>. For perforated-patch measurements, the pipette solution was supplemented with water-soluble amphotericin B (300  $\mu$ g·mL<sup>-1</sup>, Sigma-Aldrich). The perforation started shortly after seal formation and reached a steady-state level within 1–2 min. For HEK293 cells overexpressing the long isoform TRPC4 $\alpha$  or the short isoform TRPC4 $\beta$  the following pipette solution was used: 120 mM CsCl, 9.4 mM NaCl, 0.2 mM Na<sub>3</sub>GTP, 1 mM MgCl<sub>2</sub>, 7.639 mM CaCl<sub>2</sub>, 10 mM BAPTA (500 nM free Ca<sup>2+</sup>), and 10 mM Hepes (pH 7.2 with CsOH), resulting in an osmolality of about 300 mOsm·kg<sup>-1</sup>. The increased intracellular calcium concentration caused more prominent TRPC4 inward currents characterized by the typical double-rectifying current-voltage relationship. These distinct inward currents did not develop when using the standard pipette solution. Data were collected with an EPC10 patch clamp amplifier (HEKA) using the Patchmaster software. Current density voltage relations were obtained from triangular voltage ramps from -100 to +60 mV with a slope of 0.4 V·s<sup>-1</sup> applied at a frequency of 1 Hz. Data were acquired at a frequency of 5 kHz after filtering at 1.67 kHz. The current density voltage curves and the current density amplitudes at  $\pm 60$  mV were extracted at minimal or maximal currents, respectively. For single-channel measurements, HEK293 cells were seeded on culture dishes treated with poly-L-lysine. Patch pipettes made of borosilicate glass (Science Products) had resistances of 2.0–3.5 M $\Omega$  for whole-cell and 5–8 M $\Omega$  for outside-out measurements. For outside-out measurements, data were acquired at a holding potential of -60 mV with a frequency of 20 kHz after filtering at 6.67 kHz. For the evaluation of consecutive channel activity (NPO, the product of the number of channels and open probability) in 1-s steps, PC DAC 1.1.5 of Marburg University Software Team was used. Bath solutions with 100  $\mu$ M OAG contained 0.1% BSA to prevent micelle formation and to enhance solubility. To rule out side effects of 0.1% BSA and 0.1% DMSO in the OAG containing bath solution, cells were superfused before OAG administration with the control solution containing 0.1% BSA and 0.1% DMSO. The control solution never induced TRPC5 currents.

**Determination of Intracellular Calcium Concentrations and Mn<sup>2+</sup> Quenching.** Intracellular free calcium concentrations were determined in fura-2-acetox-

ymethyl ester (fura-2, 5  $\mu$ M; Sigma-Aldrich)-loaded HEK293 cells. Coverslips were mounted on the stage of a monochromator-equipped (Polychrome V, TILL Photonics) inverted microscope (Olympus IX 71 with an UPlanSApo 20 $\times$ /0.85 oil immersion objective). Fluorescence was recorded with a 14-bit EMCCD camera (IXON 885K, Andor). Fura-2 fluorescence was excited at 340 and 380 nm. Intracellular free calcium concentrations were calculated as described previously (65). For Mn<sup>2+</sup> quench experiments, transfected HEK293 cells were also loaded with fura-2. The fluorescence of fura-2 was excited at 340, 360, and 380 nm. Cells were continuously superfused at room temperature with Hepes-buffered saline containing (in millimoles) 140 NaCl, 5 KCl, 1 MgCl<sub>2</sub>, 2 CaCl<sub>2</sub>, 5 glucose, and 10 Hepes (pH 7.4 with NaOH). In Mn<sup>2+</sup> quench experiments, 200  $\mu$ M MnCl<sub>2</sub> was applied. Mn<sup>2+</sup> quench was calculated and normalized as described previously (66). Cells with basal intracellular calcium levels of  $\geq 200$  nM and with basal manganese influx rates of  $\geq 0.15\%$  per second were excluded from further analysis.

**Dynamic Intermolecular FRET.** To measure NHERF1 dissociation from the C terminus of TRPC5, intermolecular dynamic FRET between Cerulean- and eYFP-labeled proteins was measured in single cells as described previously (67). Briefly, monoclonal HEK293 cells stably expressing N-terminally Cerulean-tagged human NHERF1 (68) were cotransfected with C-terminally eYFP-tagged murine TRPC5, murine TRPC5-T972A, murine TRPC5-T972D, or with murine TRPC6. To analyze C-terminal conformational changes of TRPC5, HEK293 cells were transiently transfected with C-terminally eYFP- and eCFP-tagged TRPC5 or TRPC5-T972A in a 1:1 ratio. At 24 h after transfection, cells were seeded into six channel flow chambers ( $\mu$ -slide VI 0.1 or 0.4, Ibidi) 24 h before analysis. For analysis, cells were continuously superfused with HBS solution on the stage of an inverted microscope (IX 70, Olympus) with an UPlanSApo 100 $\times$ /1.40 oil immersion objective. Added to the bath solution were 20  $\mu$ M wortmannin, 100  $\mu$ M carbachol, 100  $\mu$ M ATP, or 100  $\mu$ M OAG. Upon excitation at 430 nm with Polychrome V (TILL Photonics) fluorescence intensities at 480  $\pm$  20 and 535  $\pm$  15 nm were measured with a dual-emission photometry system (TILL Photonics). Emission was measured as voltage of the transimpedance amplifier from the photodiodes with a frequency of 5 kHz and collected by EPC10 amplifier (HEKA) with Patchmaster software (HEKA). FRET ratios were measured as the ratio of the eYFP and eCFP/Cerulean emission.  $F_{eYFP}/F_{Cerulean}$  or  $F_{eYFP}/F_{eCFP}$  are calculated as the corrected emission intensities at 535  $\pm$  15 and 480  $\pm$  20 nm (beam splitter DCLP 505 nm) on excitation at 430 nm (beam splitter DCLP 460 nm). Excitation time was 4.6 or 5.6 ms and sampling rate was 10 or 5 Hz, respectively. Bleed through of eCFP or Cerulean into the 535-nm channel was 7%, which was determined by analyzing only eCFP or Cerulean-expressing HEK293 cells. There were no significant differences between bleed through of eCFP or Cerulean-expressing cells. Bleed through was subtracted to yield a corrected FRET ratio. Spillover of eYFP into the 480-nm channel determined by measuring eYFP-expressing cells was negligible. Stimuli were applied when steady-state conditions of both fluorescence traces were reached. Thus, correction for bleaching was not necessary. Ratio changes were further analyzed and regarded as FRET signals if the course of the single fluorescence traces developed in opposite directions. Moreover, only cells with low fluorescence intensities showing membrane staining of channel fluorescence were selected for further analysis.

**Statistical Analysis.** Data are presented as means  $\pm$  SEM. Unless stated otherwise, data were compared by a paired or unpaired Student's *t* test, if a Gaussian distribution was confirmed by applying a Shapiro-Wilk (normality) test, and significance was accepted at  $P < 0.05$ . \* $P < 0.05$ , \*\* $P < 0.01$ , \*\*\* $P < 0.001$ , n.s.  $P > 0.05$ .

**ACKNOWLEDGMENTS.** We thank Margarete Göppelt-Strübe and Lorraine Racusen for providing HKC8 cells; Carsten Cullmsee for providing HT22 cells; Dominik Oliver for providing cDNA constructs for rapamycin-induced PIP<sub>2</sub> depletion; Peter A. Friedmann for Cerulean-NHERF1 cDNA; and Laura Danner, Haoming Ren, and Joanna Zaisserer for excellent technical assistance. This work was supported by the Deutsche Forschungsgemeinschaft, Grant TRR 152.

- Riccio A, et al. (2009) Essential role for TRPC5 in amygdala function and fear-related behavior. *Cell* 137(4):761–772.
- Riccio A, et al. (2014) Decreased anxiety-like behavior and G $\alpha$ q/11-dependent responses in the amygdala of mice lacking TRPC4 channels. *J Neurosci* 34(10):3653–3667.
- Phelan KD, et al. (2013) Canonical transient receptor channel 5 (TRPC5) and TRPC1/4 contribute to seizure and excitotoxicity by distinct cellular mechanisms. *Mol Pharmacol* 83(2):429–438.

- Tai C, Hines DJ, Choi HB, MacVicar BA (2011) Plasma membrane insertion of TRPC5 channels contributes to the cholinergic plateau potential in hippocampal CA1 pyramidal neurons. *Hippocampus* 21(9):958–967.
- Greka A, Navarro B, Oancea E, Duggan A, Clapham DE (2003) TRPC5 is a regulator of hippocampal neurite length and growth cone morphology. *Nat Neurosci* 6(8):837–845.
- Tian D, et al. (2010) Antagonistic regulation of actin dynamics and cell motility by TRPC5 and TRPC6 channels. *Sci Signal* 3(145):ra77.

7. Beck B, et al. (2006) TRPC7 is a receptor-operated DAG-activated channel in human keratinocytes. *J Invest Dermatol* 126(9):1982–1993.
8. Hofmann T, et al. (1999) Direct activation of human TRPC6 and TRPC3 channels by diacylglycerol. *Nature* 397(6716):259–263.
9. Lucas P, Ukhanov K, Leinders-Zufall T, Zufall F (2003) A diacylglycerol-gated cation channel in vomeronasal neuron dendrites is impaired in TRPC2 mutant mice: Mechanism of pheromone transduction. *Neuron* 40(3):551–561.
10. Venkatachalam K, Zheng F, Gill DL (2003) Regulation of canonical transient receptor potential (TRPC) channel function by diacylglycerol and protein kinase C. *J Biol Chem* 278(31):29031–29040.
11. Otsuguro K, et al. (2008) Isoform-specific inhibition of TRPC4 channel by phosphatidylinositol 4,5-bisphosphate. *J Biol Chem* 283(15):10026–10036.
12. Trebak M, et al. (2009) Complex functions of phosphatidylinositol 4,5-bisphosphate in regulation of TRPC5 cation channels. *Pflugers Arch* 457(4):757–769.
13. Itsuki K, et al. (2014) PLC-mediated PI(4,5)P<sub>2</sub> hydrolysis regulates activation and inactivation of TRPC6/7 channels. *J Gen Physiol* 143(2):183–201.
14. Lee YM, et al. (2003) TRPC5 as a candidate for the nonselective cation channel activated by muscarinic stimulation in murine stomach. *Am J Physiol Gastrointest Liver Physiol* 284(4):G604–G616.
15. Mery L, Strauss B, Dufour JF, Krause KH, Hoth M (2002) The PDZ-interacting domain of TRPC4 controls its localization and surface expression in HEK293 cells. *J Cell Sci* 115(Pt 17):3497–3508.
16. Obukhov AG, Nowycky MC (2004) TRPC5 activation kinetics are modulated by the scaffolding protein ezrin/radixin/moesin-binding phosphoprotein-50 (EBP50). *J Cell Physiol* 201(2):227–235.
17. Tang Y, et al. (2000) Association of mammalian trp4 and phospholipase C isozymes with a PDZ domain-containing protein, NHERF. *J Biol Chem* 275(48):37559–37564.
18. Zhu MH, et al. (2005) Desensitization of canonical transient receptor potential channel 5 by protein kinase C. *Am J Physiol Cell Physiol* 289(3):C591–C600.
19. Shenolikar S, et al. (2001) N-terminal PDZ domain is required for NHERF dimerization. *FEBS Lett* 489(2–3):233–236.
20. Hall RA, et al. (1998) A C-terminal motif found in the beta2-adrenergic receptor, P2Y1 receptor and cystic fibrosis transmembrane conductance regulator determines binding to the Na<sup>+</sup>/H<sup>+</sup> exchanger regulatory factor family of PDZ proteins. *Proc Natl Acad Sci USA* 95(15):8496–8501.
21. Hall RA, et al. (1998) The beta2-adrenergic receptor interacts with the Na<sup>+</sup>/H<sup>+</sup> exchanger regulatory factor to control Na<sup>+</sup>/H<sup>+</sup> exchange. *Nature* 392(6676):626–630.
22. Hall RA, et al. (1999) G protein-coupled receptor kinase 6A phosphorylates the Na<sup>+</sup>/H<sup>+</sup> exchanger regulatory factor via a PDZ domain-mediated interaction. *J Biol Chem* 274(34):24328–24334.
23. Maudsley S, et al. (2000) Platelet-derived growth factor receptor association with Na<sup>+</sup>/H<sup>+</sup> exchanger regulatory factor potentiates receptor activity. *Mol Cell Biol* 20(22):8352–8363.
24. Weinman EJ, Hall RA, Friedman PA, Liu-Chen LY, Shenolikar S (2006) The association of NHERF adaptor proteins with g protein-coupled receptors and receptor tyrosine kinases. *Annu Rev Physiol* 68:491–505.
25. Cunningham R, Biswas R, Steplock D, Shenolikar S, Weinman E (2010) Role of NHERF and scaffolding proteins in proximal tubule transport. *Urol Res* 38(4):257–262.
26. Ghishan FK, Kiela PR (2012) Small intestinal ion transport. *Curr Opin Gastroenterol* 28(2):130–134.
27. Ritter SL, et al. (2011) GLAST stability and activity are enhanced by interaction with the PDZ scaffold NHERF-2. *Neurosci Lett* 487(1):3–7.
28. Paquet M, et al. (2006) The PDZ scaffold NHERF-2 interacts with mGluR5 and regulates receptor activity. *J Biol Chem* 281(40):29949–29961.
29. Georgescu MM, Morales FC, Molina JR, Hayashi Y (2008) Roles of NHERF1/EBP50 in cancer. *Curr Mol Med* 8(6):459–468.
30. Voltz JW, Weinman EJ, Shenolikar S (2001) Expanding the role of NHERF, a PDZ-domain containing protein adapter, to growth regulation. *Oncogene* 20(44):6309–6314.
31. Lee SJ, et al. (2011) MAGI-3 competes with NHERF-2 to negatively regulate LPA2 receptor signaling in colon cancer cells. *Gastroenterology* 140(3):924–934.
32. Lee-Kwon W, Wade JB, Zhang Z, Pallone TL, Weinman EJ (2005) Expression of TRPC4 channel protein that interacts with NHERF-2 in rat descending vasa recta. *Am J Physiol Cell Physiol* 288(4):C942–C949.
33. Semtner M, Schaefer M, Pinkenburg O, Plant TD (2007) Potentiation of TRPC5 by protons. *J Biol Chem* 282(46):33868–33878.
34. Jung S, et al. (2003) Lanthanides potentiate TRPC5 currents by an action at extracellular sites close to the pore mouth. *J Biol Chem* 278(6):3562–3571.
35. Courbebaisse M, et al. (2012) A new human NHERF1 mutation decreases renal phosphate transporter NPT2a expression by a PTH-independent mechanism. *PLoS One* 7(4):e34764.
36. Strübing C, Krapivinsky G, Krapivinsky L, Clapham DE (2001) TRPC1 and TRPC5 form a novel cation channel in mammalian brain. *Neuron* 29(3):645–655.
37. Akbulut Y, et al. (2015) (-)-Englerin A is a potent and selective activator of TRPC4 and TRPC5 calcium channels. *Angew Chem Int Ed Engl* 54(12):3787–3791.
38. Racusen LC, et al. (1997) Cell lines with extended in vitro growth potential from human renal proximal tubule: characterization, response to inducers, and comparison with established cell lines. *J Lab Clin Med* 129(3):318–329.
39. Turvey MR, Wang Y, Gu Y (2010) The effects of extracellular nucleotides on [Ca<sup>2+</sup>]<sub>i</sub> signalling in a human-derived renal proximal tubular cell line (HKC-8). *J Cell Biochem* 109(1):132–139.
40. Miller M, et al. (2011) Identification of ML204, a novel potent antagonist that selectively modulates native TRPC4/C5 ion channels. *J Biol Chem* 286(38):33436–33446.
41. Miller MR, et al. (2010) Novel Chemical Inhibitor of TRPC4 Channels (Probe Reports from the NIH Molecular Libraries Program, Bethesda, MD).
42. Davis JB, Maher P (1994) Protein kinase C activation inhibits glutamate-induced cytotoxicity in a neuronal cell line. *Brain Res* 652(1):169–173.
43. Kim BJ, Kim MT, Jeon JH, Kim SJ, So I (2008) Involvement of phosphatidylinositol 4,5-bisphosphate in the desensitization of canonical transient receptor potential 5. *Biol Pharm Bull* 31(9):1733–1738.
44. Lindner M, Leitner MG, Halaszovich CR, Hammond GR, Oliver D (2011) Probing the regulation of TASK potassium channels by PI4,5P<sub>2</sub> with switchable phosphoinositide phosphatases. *J Physiol* 589(Pt 13):3149–3162.
45. Jeon JP, et al. (2012) Selective Gαi subunits as novel direct activators of transient receptor potential canonical (TRPC)4 and TRPC5 channels. *J Biol Chem* 287(21):17029–17039.
46. Thakur DP, et al. (2016) Critical roles of G*1*o proteins and phospholipase C-δ1 in the activation of receptor-operated TRPC4 channels. *Proc Natl Acad Sci USA* 113(4):1092–1097.
47. Yoo D, et al. (2004) Assembly and trafficking of a multiprotein ROMK (Kir 1.1) channel complex by PDZ interactions. *J Biol Chem* 279(8):6863–6873.
48. Deval E, et al. (2006) Regulation of sensory neuron-specific acid-sensing ion channel 3 by the adaptor protein Na<sup>+</sup>/H<sup>+</sup> exchanger regulatory factor-1. *J Biol Chem* 281(3):1796–1807.
49. Palmada M, et al. (2005) Requirement of PDZ domains for the stimulation of the epithelial Ca<sup>2+</sup> channel TRPV5 by the NHE regulating factor NHERF2 and the serum and glucocorticoid inducible kinase SGK1. *Cell Physiol Biochem* 15(1–4):175–182.
50. Raghuram V, Hormuth H, Foskett JK (2003) A kinase-regulated mechanism controls CFTR channel gating by disrupting bivalent PDZ domain interactions. *Proc Natl Acad Sci USA* 100(16):9620–9625.
51. Kim H, et al. (2013) An essential role of PI(4,5)P<sub>2</sub> for maintaining the activity of the transient receptor potential canonical (TRPC)4β. *Pflugers Arch* 465(7):1011–1021.
52. Boulay G, et al. (1997) Cloning and expression of a novel mammalian homolog of *Drosophila* transient receptor potential (Trp) involved in calcium entry secondary to activation of receptors coupled by the Gq class of G protein. *J Biol Chem* 272(47):29672–29680.
53. Zhu X, Jiang M, Birnbaumer L (1998) Receptor-activated Ca<sup>2+</sup> influx via human Trp3 stably expressed in human embryonic kidney (HEK)293 cells. Evidence for a non-capacitative Ca<sup>2+</sup> entry. *J Biol Chem* 273(1):133–142.
54. Halaszovich CR, Zitt C, Jungling E, Luckhoff A (2000) Inhibition of TRP3 channels by lanthanides. Block from the cytosolic side of the plasma membrane. *J Biol Chem* 275(48):37423–37428.
55. Riccio A, et al. (2002) Cloning and functional expression of human short TRP7, a candidate protein for store-operated Ca<sup>2+</sup> influx. *J Biol Chem* 277(14):12302–12309.
56. Maher P, Davis JB (1996) The role of monoamine metabolism in oxidative glutamate toxicity. *J Neurosci* 16(20):6394–6401.
57. Kritis AA, Stamoula EG, Paniskaki KA, Vavilis TD (2015) Researching glutamate-induced cytotoxicity in different cell lines: A comparative/collective analysis/study. *Front Cell Neurosci* 9:91.
58. Yan HD, Villalobos C, Andrade R (2009) TRPC channels mediate a muscarinic receptor-induced afterdepolarization in cerebral cortex. *J Neurosci* 29(32):10038–10046.
59. Zhang C, Bosch MA, Rønnekleiv OK, Kelly MJ (2013) Kisspeptin activation of TRPC4 channels in female GnRH neurons requires PIP2 depletion and cSrc kinase activation. *Endocrinology* 154(8):2772–2783.
60. Zhang C, Roepke TA, Kelly MJ, Rønnekleiv OK (2008) Kisspeptin depolarizes gonadotropin-releasing hormone neurons through activation of TRPC-like cationic channels. *J Neurosci* 28(17):4423–4434.
61. Shenolikar S, Voltz JW, Cunningham R, Weinman EJ (2004) Regulation of ion transport by the NHERF family of PDZ proteins. *Physiology* 19:362–369.
62. Svobodova B, Groschner K (2016) Mechanisms of lipid regulation and lipid gating in TRPC channels. *Cell Calcium* 59(6):271–279.
63. Wang B, et al. (2010) Na/H exchanger regulatory factors control parathyroid hormone receptor signaling by facilitating differential activation of G(α) protein subunits. *J Biol Chem* 285(35):26976–26986.
64. Storch U, Forst AL, Philipp M, Gudermann T, Mederos y Schnitzler M (2012) Transient receptor potential channel 1 (TRPC1) reduces calcium permeability in heteromeric channel complexes. *J Biol Chem* 287(5):3530–3540.
65. Gryniewicz G, Poenie M, Tsien RY (1985) A new generation of Ca<sup>2+</sup> indicators with greatly improved fluorescence properties. *J Biol Chem* 260(6):3440–3450.
66. Dietrich A, et al. (2003) N-linked protein glycosylation is a major determinant for basal TRPC3 and TRPC6 channel activity. *J Biol Chem* 278(48):47842–47852.
67. Bünemann M, Frank M, Lohse MJ (2003) Gi protein activation in intact cells involves subunit rearrangement rather than dissociation. *Proc Natl Acad Sci USA* 100(26):16077–16082.
68. Ardura JA, Wang B, Watkins SC, Vilardaga JP, Friedman PA (2011) Dynamic Na<sup>+</sup>/H<sup>+</sup> exchanger regulatory factor-1 association and dissociation regulate parathyroid hormone receptor trafficking at membrane microdomains. *J Biol Chem* 286(40):35020–35029.